Dual Role of Electron-Accepting Metal-Carboxylate Ligands: Reversible Expansion of Exciton Delocalization and Passivation of Nonradiative Trap-States in Molecule-like CdSe Nanocrystals

Katie N. Lawrence,[†] Poulami Dutta,[‡] Mulpuri Nagaraju,[†] Meghan B. Teunis,[†] Barry B. Muhoberac,[†] and Rajesh Sardar*,[†,§]

[†]Department of Chemistry and Chemical Biology, Indiana University−Purdue University Indianapolis, 402 N. Blackford Street, Indianapolis, Indiana 46202, United States

[‡]Department of Chemistry, Michigan State University, 578 South Shaw Lane, East Lansing, Michigan 48824, United States

[§]Integrated Nanosystems Development Institute, Indiana University−Purdue University Indianapolis, 402 N. Blackford Street, Indianapolis, Indiana 46202, United States

S *Supporting Information*
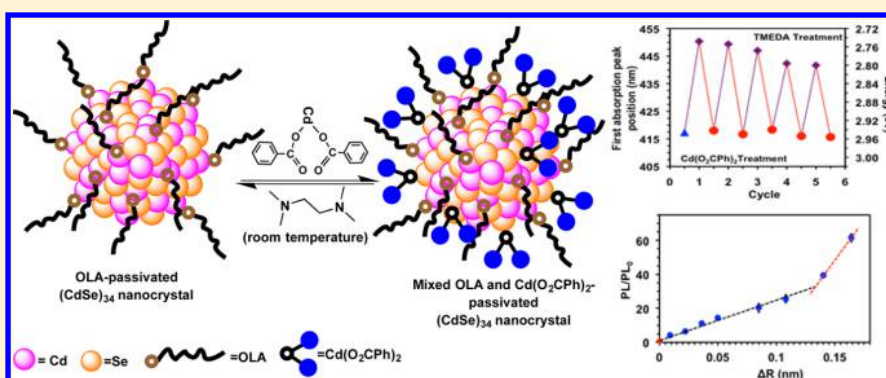
ABSTRACT: This paper reports large bathochromic shifts of up to 260 meV in both the excitonic absorption and emission peaks of oleylamine (OLA)-passivated molecule-like (CdSe)$_{34}$ nanocrystals caused by postsynthetic treatment with the electron accepting Cd(O$_2$CPh)$_2$ complex at room temperature. These shifts are found to be reversible upon removal of Cd(O$_2$CPh)$_2$ by N,N,N',N'-tetramethylethylene-1,2-diamine. ^{1}H NMR and FTIR characterizations of the nanocrystals demonstrate that the OLA remained attached to the surface of the nanocrystals during the reversible removal of Cd(O$_2$CPh)$_2$. On the basis of surface ligand characterization, X-ray powder diffraction measurements, and additional control experiments, we propose that these peak red shifts are a consequence of the delocalization of confined exciton wave functions into the interfacial electronic states that are formed from interaction of the LUMO of the nanocrystals and the LUMO of Cd(O$_2$CPh)$_2$, as opposed to originating from a change in size or reorganization of the inorganic core. Furthermore, attachment of Cd(O$_2$CPh)$_2$ to the OLA-passivated (CdSe)$_{34}$ nanocrystal surface increases the photoluminescence quantum yield from 5% to an unprecedentedly high 70% and causes a 3-fold increase of the photoluminescence lifetime, which are attributed to a combination of passivation of nonradiative surface trap states and relaxation of exciton confinement. Taken together, our work demonstrates the unique aspects of surface ligand chemistry in controlling the excitonic absorption and emission properties of ultrasmall (CdSe)$_{34}$ nanocrystals, which could expedite their potential applications in solid-state device fabrication.

INTRODUCTION

The surface ligand chemistry of semiconductor nanocrystals has profound influence on their optoelectronic properties.[1−5] Such properties can be successfully tailored by selective surface chemistry manipulation to achieve large photoluminescence quantum yield (PLQY),[1,6−11] high carrier mobility,[12−16] and fast charge transport[17−20] to facilitate optoelectronic and photovoltaic device fabrication. Surface ligands are generally introduced during the colloidal synthesis of nanocrystals;[21−24] however, most of the ligands, long-chain aliphatic amines and phosphines (neutral 2-electron donating L-type)[25,26] and long-

chain aliphatic carboxylates and phosphonates (1-electron donating X-type),[25,26] are insulating in nature. Therefore, in order to enhance the electrochemical[27−30] and charge transport properties,[19,31−35] and biological imaging detection of nanocrystals,[36−39] postsynthetic surface ligand exchange is routinely carried out. The ligand exchange reaction strongly affects the emission properties (PLQY and PL lifetime)[9,10,40−42] and excitonic absorption characteristics of nanocrystals.[2,43] Recently

Weiss and co-workers,[43,44] our group,[45,46] and others[47] have shown that postsynthetic ligand exchange of CdSe and/or CdS nanocrystals with X-type ligands induces the delocalization of quantum-confined holes causing a red-shift in the first excitonic absorption peak, which can be characterized as an "increase the confinement box size".[48,49] However, such change in the optical properties was found to be irreversible. In this article, we report for the first time that the postsynthetic surface ligand treatment of oleylamine (OLA)-passivated "molecule-like" $(CdSe)_{34}$ nanocrystals with the 2-electron accepting Z-type ligand Cd(benzoate)$_2$ $((Cd(O_2CPh)_2))$: (1) produces a mixed ligand-passivated nanocrystal $((CdSe)_{34}(OLA) Cd(O_2CPh)_2))$, and (2) induces a red-shift of the excitonic absorption and emission peaks that can be restored upon removal of $Cd(O_2CPh)_2$ through N,N,N',N'-tetramethylethylene-1,2-dia-mine (TMEDA) treatment (Scheme 1) with the red-shift caused by exciton delocalization into the ligand monolayer through hybrid orbitals that are characteristic of both nanocrystal and ligand.

Scheme 1. Reversible Surface Modification of OLA-Passivated $(CdSe)_{34}$ Nanocrystal With $Cd(O_2CPh)_2$ Complex[a]
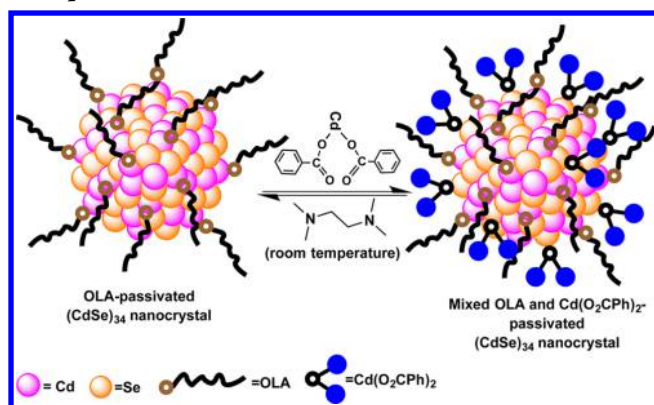
[a]The illustration of $(CdSe)_{34}$ nanocrystal structure does not correspond to the actual core-cage structure. The brown rings represent the amine headgroup of OLA; the black rings and blue dots represent Cd and the phenyl ring of $Cd(O_2CPh)_2$. Interaction between TMEDA and $Cd(O_2CPh)_2$ results in formation of the (κ^2-TMEDA) $(Cd(O_2CPh)_2)$ complex and detaches $Cd(O_2CPh)_2$ from the surface of the nanocrystals.[25]

In contrast to X-type ligand exchange in which *irreversible* change in the optical spectra has always been previously observed,[43–47] Buhro and co-workers very recently (during the course of our research) reported *reversible* shifts of 140 meV in the absorption and emission peaks of two-dimensional CdSe and CdS quantum belts upon fully exchanging L-type ligands (octylamine) with the Z-type ligands $(Cd(oleate)_2)$.[50] The shift in optical spectra was attributed to a combination of changes in strain state (structural relaxation of the inorganic core) and exciton delocalization. The magnitude of change in the confinement dimension is remarkably large considering that only an ~4 meV change was observed in the absorption spectra by Owen and co-workers for CdSe nanocrystals (>2.0 nm diameter) under similar experimental conditions.[25] However, a reversible change in the confinement dimension of zero-dimensional semiconductor nanocrystals that is solely due to delocalization of excitons upon attachment of metal-complexes without compromising the original surface chemistry of the

nanocrystals has not yet been demonstrated. In this paper, we report that attachment and detachment of $Cd(O_2CPh)_2$ to surface Se sites of $(CdSe)_{34}$ nanocrystals without displacing the original OLA attached to the surface Cd sites produces a reversible change in the nanocrystal absorption and emission peaks of up to 260 meV for at least five cycles.

Our experimental results and proposed molecular orbital (MO) theory of nanocrystal-metal complexes demonstrate that the reversible change in the optical spectra of mixed OLA- and $Cd(O_2CPh)_2$-passivated $(CdSe)_{34}$ nanocrystals is not controlled by change in dimension, crystal structure or strain states. It is, however, a consequence of delocalization of excitons *into* hybrid MOs that are formed by the interaction of LUMOs of OLA-passivated $(CdSe)_{34}$ nanocrystals and LUMOs of $Cd(O_2CPh)_2$. The wave function delocalization process is further supported by the 3-fold increase in PL lifetime.[11,51] Furthermore, our particular surface passivation increases the PLQY from 5% to 70% (see Experimental Section for detail PLQY calculation), which is the highest PLQY reported in the literature for such ultrasmall semiconductor nanocrystals,[7,52–59] and increases the radiative rate constant (k_r) by 4.3 fold, thus, illustrating the dual role of $Cd(O_2CPh)_2$ in both spectral modulation and trap state passivation.

Taken together, our results provide new insights into how optoelectronic properties can be controlled through post-synthetic surface modification without replacing the original surface ligands on the nanocrystal. Furthermore, this research provides a rational approach to obtaining the desired optoelectronic properties of semiconductor nanocrystals through selective surface passivation without changing their size, shape, or inorganic core composition.

■ RESULTS AND DISCUSSION

Surface Treatment of OLA-Passivated Molecule-like $(CdSe)_{34}$ Nanocrystals with $Cd(O_2CPh)_2$. We use OLA-coated, molecule-like $(CdSe)_{34}$ nanocrystals with core-cage structure of $(CdSe)_6(CdSe)_{28}$[60,61] as our model system for the study of surface ligand chemistry-dependent optoelectronic properties for several reasons. (1) These magic-sized nano-crystals are thermodynamically very stable,[61–64] thus changes in their crystallographic structure during the ligand exchange reaction is unlikely. (2) With nanocrystals in the ultrasmall size range, the majority of the atoms reside at the nanocrystal surface.[65,66] Therefore, even a minor variation in their surface ligand chemistry will have profound effects on their optoelectronic properties, as compared to larger nanocryst-als.[43,46,57,67–69] (3) The L-type ligand OLA binds to surface Cd sites[25] leaving the Se sites unpassivated, which can then be passivated with Z-type ligands (e.g., metal-carboxylate com-plexes) *without displacing the OLA but still changing the surface chemistry of the original nanocrystals.* Afterward we anticipate that the Z-type ligand can be removed from the surface of the nanocrystals via a ligand exchange procedure using a different L-type ligand (Scheme 1).[25] (4) We expect that the surface ligand interaction has the potential to dramatically alter nanocrystal electronic structure and dictate nanocrystal function substantially more than would be found through ligand interactions with larger nanocrystals (>2.0 nm diameter), because smaller nanocrystals have a larger surface-to-volume ratio that results in a higher relative density of surface orbitals (e.g., HOMOs and LUMOs), behaving more similarly to isolated molecules. Nanocrystal surface orbitals readily interact

with the MOs of surface ligands in a process called interfacial orbital mixing.[43,44,70,71]

The synthesis of OLA-passivated molecule-like $(CdSe)_{34}$ nanocrystals was performed according to our published procedure.[7] The blue lines in Figure 1 show that the lowest
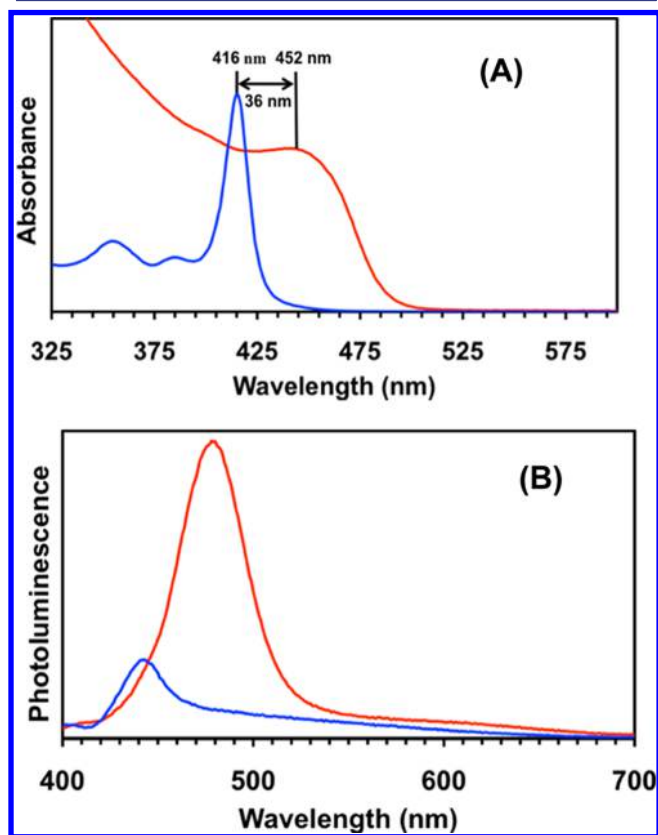

Figure 1. Absorption (A) and emission (B) spectra (in toluene) of purified OLA-passivated $(CdSe)_{34}$ nanocrystals prior to (blue lines) and after (red lines) ex situ treatment with $Cd(O_2CPh)_2$ at room temperature. The emission spectra were collected at 380 nm excitation wavelength.

energy absorption and band-edge emission peaks appear at 416 and 435 nm, respectively. The sharp initial absorption peak (fwhm ~12 nm) at this wavelength confirms the formation of nearly monodispersed $(CdSe)_{34}$ nanocrystals.[61,62] In order to investigate surface ligand-dependent optical properties, a toluene solution of OLA-passivated purified nanocrystals was treated with $Cd(O_2CPh)_2$ and stirred under N_2 atmosphere for 24 h at room temperature. All details of the surface modification procedures are provided in the Experimental Section. This reaction mixture was centrifuged to remove free $Cd(O_2CPh)_2$ and produced a clear yellow supernatant. The nanocrystals were purified with solvent-assisted precipitation and then dissolved in toluene which produced a clear yellow solution that displays a 36 nm (240 ± 12 meV) red shift with fwhm of ~40 nm in the lowest energy absorption peak (Figure 1A, red line). The shift of 240 meV in the absorption peak upon modification of our L-type ligand passivated nanocrystals with this metal-carboxylate complex is the largest shift reported in the literature for semiconductor nanocrystals with a Z-type ligand.[25,50]

Along with changes in the absorption peak, we also observe a 43 nm (260 ± 9 meV) red-shift (Figure 1B, red line) in the band-edge emission peak and peak broadening. In the event of

electronic coupling between the nanocrystals and their surface passivating ligand shell, their results in delocalization of exciton wave functions from nanocrystals into their ligand monolayer. In the solution state upon continuous random motion of nanocrystals they can transiently interact leading to variable overlap and entanglement of their wave functions. Thus, there is creation of collective electronic states (mini bands) and an increase in the confinement box size. The result is a broadening of the absorption and PL peaks of nanocrystals in solution that is closely related to literature reports in which delocalization takes place either in solution or thin-films.[72−77] However, one would expect larger delocalization of wave functions in films because of their smaller internanocrystals spacing, resulting in a more significant broadening of the peak than found in solution-state electronic interactions, as shown in the literature.[72−77] Moreover, Buhro and co-workers[50] reported a similar broadening in absorption peaks for CdSe and CdS quantum belts upon exchanging long-chain primary amines with (Cd-(oleate)$_2$). Importantly, a substantial increase in the band-edge emission peak intensity (14-fold increase in PLQY) and PL lifetime (3.3 fold increase in τ) are observed after treatment with $Cd(O_2CPh)_2$, which is due a combination of passivation of nonradiative trap states and relaxation of exciton confinement.[11,43,44,46,47,50,78] Therefore, we propose that the observed spectra characteristics, i.e., the (1) red-shifts in the absorption and emission peaks, (2) broadening of absorption peaks, (3) increase in emission peak intensity, and (4) enhancement of k_r, are all caused by a combination of delocalization of the exciton wave functions and trap state passivation of $(CdSe)_{34}$ nanocrystals as opposed to a change in nanocrystal size (mechanism (i)) or strain states (mechanism (ii)), as will be discussed below.

Binding of Z-Type Ligands. To precisely assess the $Cd(O_2CPh)_2$-induced change in the optical properties of OLA-passivated $(CdSe)_{34}$ nanocrystals, it is important to characterize their surface ligand chemistry. On the basis of our predicted model of surface structure of these nanocrystals (Scheme 1), the ligand OLA (L-type) is attached to the surface Cd sites while surface Se sites remain unpassivated. Addition of the ligand $Cd(O_2CPh)_2$ (Z-type) is expected to passivate the Se sites without replacing the OLA. Testing our surface model is important in that it is different than recent reports by the Buhro[50] and Owen[25] groups in which these authors have concluded that addition of Z-type ligands completely displaced L-type ligands from the surface of CdSe nanocrystals. To confirm our model, $Cd(O_2CPh)_2$-treated OLA-passivated $(CdSe)_{34}$ nanocrystals were analyzed by ^1H NMR and FTIR spectroscopy (see Supporting Information Figures S1 and S2, respectively). In the NMR analysis the nanocrystals display broad vinyl proton ($-CH=CH-$) and aromatic proton (-ortho) signals at 5.35 and 8.12 ppm, which originate from OLA and $Cd(O_2CPh)_2$, respectively. The NMR analysis shows a ratio of 1:1 between vinyl and aromatic ortho protons. According to DFT calculations, 28 surface Cd and 28 surface Se sites are available on $(CdSe)_{34}$ nanocrystals. Since amine can only bind to Cd sites, a maximum of 28 OLAs could attach to the surface of a $(CdSe)_{34}$ nanocrystal. However, experimental work by Wang et al.[79] showed that 18 amines can bind to this nanocrystal. On the basis of our ^1H NMR analysis, 9 $Cd(O_2CPh)_2$ ligands are bound to the surface. Our energy dispersive spectroscopic (EDS) characterization (data not shown) of OLA-passivated $(CdSe)_{34}$ nanocrystals before and after $Cd(O_2CPh)_2$ treatment shows Cd/Se ratios of 1:1 and

1.23:1, respectively, indicating an average of 8 Cd(O$_2$CPh)$_2$ ligands attach onto the surface in agreement with the NMR data. The FTIR analysis shows carboxylate group (−COO$^-$) stretch modes along with N−H stretches from the primary amine OLA. These analyses unequivocally support the mixed surface ligation of our nanocrystals and the resulting formation of [(CdSe)$_{34}$(OLA) (Cd(O$_2$CPh)$_2$)]. As discussed above, the increased emission peak intensity after Cd(O$_2$CPh)$_2$ treatment indicates its attachment to the surface Se sites while OLA remains bound to surface Cd sites. Below we address in detail the various mechanisms that could cause our observed spectral changes.

Mechanism (i): Change in the Inorganic Core Size. Our observed red-shift of 260 meV in the absorption spectra of OLA-passivated (CdSe)$_{34}$ nanocrystals upon treatment with Cd(O$_2$CPh)$_2$ could be caused by Ostwald ripening growth of the original nanocrystals, resulting in an increase in size and thus in confinement dimension. Although Ostwald ripening growth of thermodynamically stable (CdSe)$_{34}$ nanocrystals is unlikely at room temperature, addition of Cd(O$_2$CPh)$_2$ could trigger such a process. Thus, we performed transmission electron microscopic (TEM) analysis to determine the diameter of the (CdSe)$_{34}$ nanocrystals before and after Cd(O$_2$CPh)$_2$ attachment (see Figure S3). The original OLA-passivated (CdSe)$_{34}$ nanocrystals are 1.6 ± 0.2 nm in diameter[7] and no noticeable change in diameter is observed after Cd(O$_2$CPh)$_2$ attachment. Moreover, the nanocrystals remained well disperse on the TEM grid. In this context, our observed red-shift in the lowest energy absorption peak of (CdSe)$_{34}$ nanocrystals after Cd(O$_2$CPh)$_2$ treatment to 452 nm corresponds to a final diameter of 2.0 nm, based on a generally used empirical formula.[80] Precisely quantifying such a small difference in diameter (0.4 nm) by TEM is extremely challenging, and thus proving our hypothesis that attachment of Cd(O$_2$CPh)$_2$ to OLA-passivated (CdSe)$_{34}$ nanocrystals does not change the actual core dimension using TEM is difficult. An alternative way to prove size retention of (CdSe)$_{34}$ nanocrystals after treatment and that the 36 nm red-shift of the absorption peak is due to attachment of Cd(O$_2$CPh)$_2$ is through reversing the absorption peak shift by detaching Cd(O$_2$CPh)$_2$ and not finding an accumulating increase in wavelength with each cycle.

We further evaluated the possibility of growth of OLA-passivated (CdSe)$_{34}$ nanocrystals from treatment by Cd-(O$_2$CPh)$_2$ using a simple mathematic model. According to the empirical formula reported by Peng and co-workers,[80] CdSe nanocrystals displaying a UV−visible absorption peak at 416 nm should have a radius of 0.80 nm, which is similar to that found in our TEM analysis (Figure S3). As shown in Figure 1A, after treatment with Cd(O$_2$CPh)$_2$ the peak shifts to 452 nm corresponding to a calculated radius of 0.97 nm. In the event that Cd(O$_2$CPh)$_2$ treatment caused Ostwald ripening growth, the deposition of a monolayer of Cd would increase the radius by 0.26 nm, which is the Cd−Se bond distance.[41] Therefore, according to the empirical formula, the 0.17 nm increase of our OLA-passivated (CdSe)$_{34}$ nanocrystals upon treatment with Cd(O$_2$CPh)$_2$ should correspond to the deposition of 65% of a monolayer of Cd. However, our ^{1}H NMR and EDS analyses suggest that ∼30% of the nanocrystal surface is covered by Cd(O$_2$CPh)$_2$. Thus, the wavelength shift is greater than predicted by the percent coverage. More importantly, deposition of Cd would permanently increase the size of the nanocrystals and shift the absorption peak to higher wavelength in a manner that is not reversible after removal of the ligand.

We have shown fully reversible absorption and emission peaks of OLA-passivated (CdSe)$_{34}$ nanocrystals upon detachment of Cd(O$_2$CPh)$_2$.

Optical Spectroscopy: Reversible Modulation of the Absorption Peak of (CdSe)$_{34}$ Nanocrystals. We used a ligand exchange procedure similar to that reported in the literature[25] to remove Cd(O$_2$CPh)$_2$ from the surface of (CdSe)$_{34}$ nanocrystals by treatment with TMEDA. As mentioned previously, a 36 nm red-shift in the absorption peak of OLA-passivated (CdSe)$_{34}$ nanocrystals is observed after treatment with Cd(O$_2$CPh)$_2$. Figure 2A illustrates that
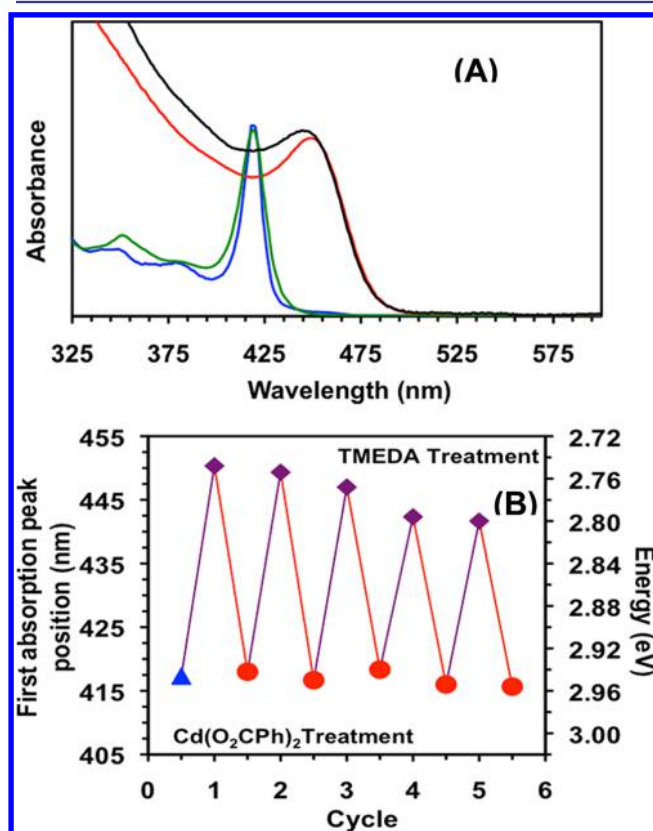

Figure 2. (A) Room temperature absorption spectra (in toluene) of purified OLA-passivated (CdSe)$_{34}$ nanocrystals after synthesis (blue line), after binding Cd(O$_2$CPh)$_2$ (red line), after treatment with TMEDA (green line), and after rebinding Cd(O$_2$CPh)$_2$ (black line). (B) Reversibility of the lowest energy absorption peak position of purified OLA-passivated (CdSe)$_{34}$ nanocrystals (blue triangle) after repeatedly binding Cd(O$_2$CPh)$_2$ (purple diamonds) and removing Cd(O$_2$CPh)$_2$ by TMEDA treatment (red dots). Over time, the peak position does not fully reverse, which could be due to change in the surface chemistry caused by multiple purifications.

TMEDA treatment of our mixed ligand-passivated nanocrystals causes an ∼35 nm blue-shift in the absorption spectrum. Importantly, the peak retains the spectral shape (fwhm ∼13 nm) of the original OLA-passivated (CdSe)$_{34}$ nanocrystals. When the purified (CdSe)$_{34}$ nanocrystals are again treated with Cd(O$_2$CPh)$_2$, an average 35 nm red-shift in the absorption peak position is observed. As shown in Figure 2B and Figure S4, we observe this reversible change in the absorption and emission peak positions over at least 5 cycles due to attachment and detachment of Cd(O$_2$CPh)$_2$ from the surface of the OLA-passivated (CdSe)$_{34}$ nanocrystals.

^{1}H NMR Spectroscopy: Detachment of the Z-Type Ligand $Cd(O_2CPh)_2$. We used in situ ^{1}H NMR spectroscopy to monitor the $Cd(O_2CPh)_2$ removal from the surface of $((CdSe)_{34}(OLA)Cd(O_2CPh)_2))$ nanocrystals. Figure 3 shows

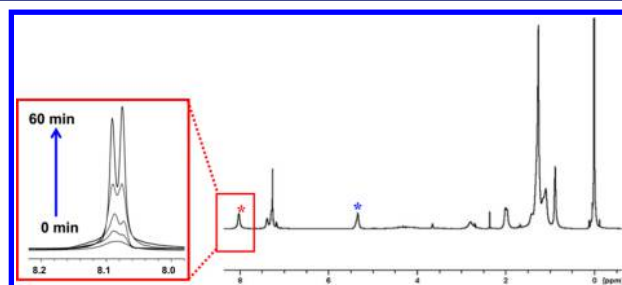**Figure 3.** ^{1}H NMR spectrum of purified OLA-passivated $(CdSe)_{34}$ nanocrystals after binding of $Cd(O_2CPh)_2$ and inset showing time-dependence from TMEDA treatment. The appearance of broad aromatic (red star) and vinyl (blue star) proton signals from $Cd(O_2CPh)_2$ and OLA, respectively, suggests that the nanocrystal surface is passivated with these two ligands. The expanded spectra in the inset demonstrate the temporal evolution of sharp aromatic peaks at ~8.1 ppm after TMEDA treatment of nanocrystals that have mixed (OLA) and $Cd(O_2CPh)_2$ passivation.

the time-dependent ^{1}H NMR spectra of the aromatic *ortho* proton signals of $Cd(O_2CPh)_2$ at 8.12 ppm after TMEDA treatment. The broad aromatic signal, which appears from a combination of spin−spin relaxation and dipole broadening,[59,81,82] becomes sharper and increases in intensity. Our experimental result is in agreement with a previous report demonstrating removal of Z-type ligands from the surface of CdSe nanocrystals upon treatment with L-type ligands.[25] Importantly, vinyl resonance signals ($-CH{=}CH-$) at 5.35 ppm from OLA remain broad even after TMEDA treatment (Figure S5A), suggesting that OLA is still present on the surface of the $(CdSe)_{34}$ nanocrystals. Furthermore, time-dependent ^{1}H NMR spectra show vinyl peak broadness and constant peak area throughout the TMEDA treatment of 1 h (see Figure S5B). Moreover, the total number of bound and free $Cd(O_2CPh)_2$ present in the nanocrystal solution is found to be constant during the TMEDA treatment (Figure S5C). Taken together, addition of TMEDA to the $(CdSe)_{34}(OLA)$-$Cd(O_2CPh)_2$ nanocrystals results in formation of a TMEDA-$Cd(O_2CPh)_2)$ complex, which weakens the interaction between Cd from $Cd(O_2CPh)_2)$ and the Se sites of the $(CdSe)_{34}$ nanocrystals and removes $Cd(O_2CPh)_2$ from their surface.

FTIR Spectroscopy: Reversible Change in Surface Ligand Chemistry. To further elucidate the mechanism of control of relaxation of exciton confinement by manipulating surface passivating ligands of molecule-like $(CdSe)_{34}$ nanocrystals, we used FTIR spectroscopy to characterize surface ligand chemistry and specifically the reversible exchange of $Cd(O_2CPh)_2$. After different ligand treatments and before each spectroscopic measurement, the nanocrystals were purified through a solvent-assisted precipitation technique to remove free and/or loosely bound ligands. Figure 4A illustrates the FTIR spectra of OLA-passivated $(CdSe)_{34}$ nanocrystals (a, black curve) in which the characteristic N−H stretch in the range 3400−3000 cm^{-1} and the N−H bending mode at 1581 cm^{-1} (Figure 4B) appear, confirming the presence of the primary amine OLA passivating the nanocrystal surface.[83] After the $Cd(O_2CPh)_2$ treatment (b, red curve), new asymmetric (1518 cm^{-1}) and symmetric (1388 cm^{-1}) stretch vibrations
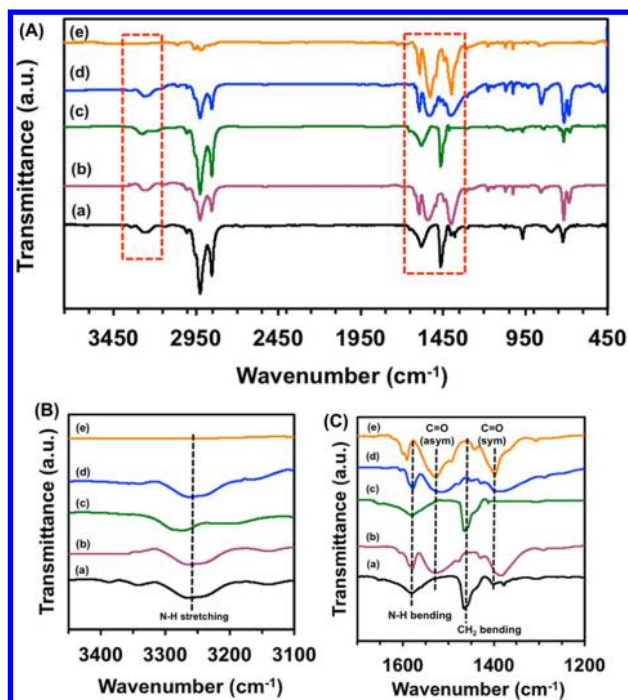

Figure 4. (A) FTIR spectra of purified OLA-passivated $(CdSe)_{34}$ nanocrystals (a), and after (b) binding of $Cd(O_2CPh)_2$, (c) displacement of by TMEDA, and (d) the second addition of $Cd(O_2CPh)_2$. Pure $Cd(O_2CPh)_2$ (e). (B) Expanded FTIR of N−H stretch region in the range of 3400−3000 cm^{-1}, and (C) expanded N−H bending mode, asymmetric stretch and symmetric stretch of the carboxylate group. Both expanded regions (B and C) are highlighted by dotted red boxes in A.

from the carboxylate group ($-COO^-$) develop (Figure 4C). The separation between these two vibrations is 130 cm^{-1}, which suggests $-COO^-$ attachment to Cd^{2+} through a chelating bidentate interaction.[2,52,84] Importantly, both the asymmetric and symmetric vibrations red-shift from 1527 (~9 cm^{-1}, 39 nm) and 1397 cm^{-1} (~9 cm^{-1}, 46 nm), respectively, along with peak broadening from that of pure $Cd(O_2CPh)_2$ (e, orange curve), which suggests that the interaction between $-COO^-$ and Cd^{2+} weakens due to their attachment to the surface Se sites. Furthermore, the presence of N−H stretching and N−H bending modes indicates mixed surface ligation, and the addition of $Cd(O_2CPh)_2$ does not replace OLA, as had been demonstrated in the literature.[25,50] The addition of TMEDA to the $(CdSe)_{34}(OLA)Cd(O_2CPh)_2$ nanocrystals removes the characteristic $-COO^-$ vibration modes (c, green curve), which reappear after the addition of $Cd(O_2CPh)_2$ to the nanocrystals. Moreover, no noticeable change in the position of the N−H bending mode (Figure 4B) is indicative of the attachment of $Cd(O_2CPh)_2$ to the inorganic core of the nanocrytal and not to the $-NH_2$ group of OLA through hydrogen bonding.[83]

We further tested whether a reversible change in the optical spectra could be achieved upon treatment of $(CdSe)_{34}$ nanocrystals in which surface Se sites are already passivated with the $Cd(O_2CPh)_2$ complex. We prepared mixed Cd-(sterate)$_2$-, hexadecylamine (HDA)-, and trioctylphosphine (TOP)-passivated $(CdSe)_{34}$ nanocrystals,[85] which display a characteristic absorption peak at 415 nm (Figure S6). According to the literature, the nanocrystal surface is passivated with a mixture of all three ligands, and in particular, HDA and

TOP are attached to surface Cd and Se sites, respectively.[8,25,86−88] A negligible change (~14 meV red-shift) in the lowest energy absorption peak position is observed over a 24 h period after addition of $Cd(O_2CPh)_2$ at room temperature. Consistent with this result is that replacement of TOP at the surface Se sites by $Cd(O_2CPh)_2$ and formation of new Se−$Cd(O_2CPh)_2$ attachment on $(CdSe)_{34}$ nanocrystals is very unlikely due to strength of the TOP-Se interaction, which in addition would result in no major change in the confinement dimension.

Mechanism (ii): Changes in the Strain States. Strongly quantum confined ultrasmall $(CdSe)_{34}$ nanocrystals have a very large surface area and radius of curvature as compared to larger nanocrystals (>2.0 nm diameter). Therefore, small changes in their surface ligand chemistry could have significant influence on their strain states, resulting in spectral shifts during Z-type ligand exchange, as opposed to larger nanocrystals (>2.0 nm diameter).[43,46] To further validate our hypothesis that attachment of $Cd(O_2CPh)_2$ to OLA-passivated $(CdSe)_{34}$ nanocrystals does not change strain and that the observe red-shift in the absorption peak position is due to exciton wave function delocalization, we performed a control experiment in which $Cd(nonanoate)_2$ was used instead of $Cd(O_2CPh)_2$ in an ex situ ligand exchange reaction to eliminate possible delocalization. In addition, we used $Cd(nonanoate)_2$ as the Z-type ligand instead of the widely used $Cd(oleate)_2$[25,50,89] so that the identity of the surface bound ligands can be investigated by ^{1}H NMR spectroscopy without the overlapping $-CH=CH-$ proton signals of OLA and oleic acid. Furthermore, both Cd-$(nonanoate)_2$ and $Cd(O_2CPh)_2$ are insoluble in the exchange solvent toluene, thus allowing us to use the same ligand exchange conditions.

Figure S7 illustrates the almost identical UV−visible absorption spectra of OLA-passivated $(CdSe)_{34}$ nanocrystals before and after treatment with $Cd(nonanoate)_2$ and shows there is no shift in the peak position. The ^{1}H NMR spectrum shows a broad $-CH=CH-$ proton signal at 5.35 ppm from OLA and a $CO-CH_2-$ proton signal at 2.38 ppm from nonanoate (Figure S8), implying the nanocrystal surface is passivated by these two ligands. The NMR analysis also indicates a 1:1 ratio of OLA:$Cd(nonanoate)_2$ present on the surface of $(CdSe)_{34}$ nanocrystals similar to our mixed OLA- and $Cd(O_2CPh)_2$-passivated nanocrystals. In addition, FTIR analysis (Figure S9) of the same sample demonstrates the formation of mixed OLA- and $Cd(nonanoate)_2$-passivated $(CdSe)_{34}$ nanocrystals. Upon $Cd(nonanoate)_2$ treatment, a significant increase in PLQY of 46% is observed, which together with the NMR and FTIR data strongly support the binding of $Cd(nonanoate)_2$ to surface Se sites and thus passivation of nonradiative trap states.[52] Our PLQY data are in agreement with the work by Rosenthal and co-workers in which postsynthetic surface ligand treatment of ultrasmall CdSe nanocrystals resulted in an increase in PLQY from ~3% to 45%.[8] The authors stated that such a dramatic increase in PLQY is a consequence of passivation of nonradiative surface trap states. Nevertheless, the PLQY of our mixed OLA- and $Cd(nonanoate)_2$-passivated $(CdSe)_{34}$ nanocrystals is nearly 25% lower than we found with the OLA- and $Cd(O_2CPh)_2$ passivated nanocrystals. Although the chemical structure of nonanoate and benzoate is different, their mode of binding to Cd^{2+} and the interaction of $Cd(nonanoate)_2$ and $Cd(O_2CPh)_2$ with the surface Se sites of CdSe nanocrystals are expected to be very similar. The ratio of these two Cd complexes to OLA

on the CdSe nanocrystal surface is also found to be the same as determined from the NMR analysis. Therefore, the higher PLQY for $Cd(O_2CPh)_2$ is considered to stem from a combination of the passivation of nonradiative trap states and the *delocalization of exciton wave functions*.

At present, we are not certain of the explanation as to why CdSe quantum belts display an ~140 meV absorption peak shift caused by $Cd(oleate)_2$ attachment.[50] Our ultrasmall $(CdSe)_{34}$ nanocrystals that have a large surface area similar to quantum belts show no change in their lowest energy absorption peak with $Cd(nonanoate)_2$ attachment, even though both ligands are almost identical structurally and are Z-type. One possible explanation is that in the case of CdSe quantum belts, octylamine is fully exchanged by $Cd(oleate)_2$ causing the inorganic crystal lattice to undergo a significant contraction process. In our investigation, $Cd(nonanoate)_2$ is attached onto the $(CdSe)_{34}$ nanocrystal surface without replacing the bound OLA, and thus a lattice contraction as suggested for CdSe quantum belts might not take place. Furthermore, X-ray diffraction (XRD) analysis of OLA-passivated $(CdSe)_{34}$ nanocrystals shows three peaks along the (100), (002), and (101) reflections (see Figure 5), which represent the wurtzite crystals
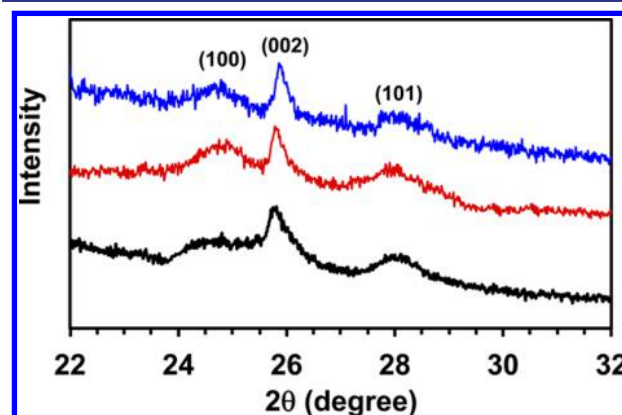

Figure 5. XRD pattern of purified OLA-passivated $(CdSe)_{34}$ nanocrystals (black line), and after binding of $Cd(O_2CPh)_2$ (red line), and removal by TMEDA (blue line).

structure in agreement with the literature.[7,54] After Cd-$(O_2CPh)_2$ treatment, a very slight change of $2\theta = 0.09°$ in the (002) peak of OLA-passivated $(CdSe)_{34}$ nanocrystals ($2\theta = 25.72°$) is observed. The differences in lattice strain due to modification of surface ligation would result in a significantly larger change in the diffraction planes ($2\theta = 1°$), as reported by Buhro and co-workers.[50] XRD analysis therefore suggests no changes in the crystal strain state caused by the attachment of $Cd(O_2CPh)_2$ to the surface of our $(CdSe)_{34}$ nanocrystals.

The delocalization of exciton wave functions of the CdSe quantum belts into the $Cd(oleate)_2$ monolayer results in an ~90 meV red-shift in the lowest energy absorption peak.[50] We do not observe a shift for our OLA-passivated $(CdSe)_{34}$ nanocrystals after $Cd(nonanoate)_2$ treatment, indicating no wave function delocalization. We believe that an appropriate energetic alignment between the Z-type ligand and nanocrystal MOs is critical for delocalization of exciton wave functions as discuss below. No noticeable changes in the XRD peak positions are observed for our OLA-passivated $(CdSe)_{34}$ nanocrystals upon $Cd(nonanoate)_2$ and $Cd(O_2CPh)_2$ treatment, which taken together, suggests that mechanism (ii) does not play a role in the shift of the lowest energy absorption peak
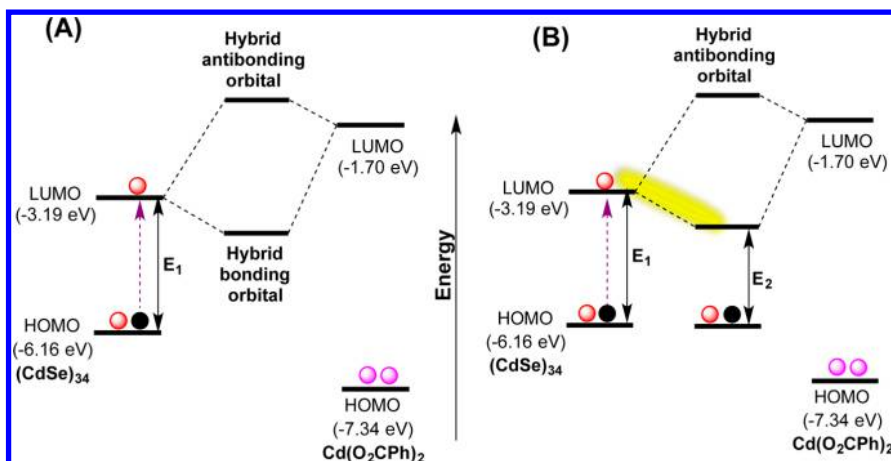
Figure 6. (A) Simplified MO diagram of an OLA-passivated $(CdSe)_{34}$ nanocrystal upon its interaction with the ligand $Cd(O_2CPh)_2$. Starting from the ground state, photoexcitation of an electron (dotted purple arrow) from the HOMO to the LUMO will create a hole (black dot). In the excited state when the LUMO of the nanocrystal is half-filled it can act as a π-donor and Lewis acid with $Cd(O_2CPh)_2$ acting as a π-acceptor with its LUMO. On the basis of MO theory,[93] one-half-filled and one completely empty orbital can interact resulting in formation of hybrid bonding and anitibonding MOs. (B) Schematic representation of the electron wave function delocalization (yellow color) into the hybrid bonding orbital, thus increasing the size of the "confinement box", which results in a red-shift in the lowest energy absorption peak $(E_2 < E_1)$. The images are not to scale. The HOMO and LUMO energy positions of $Cd(O_2CPh)_2$ are determined from DFT calculations and the $(CdSe)_{34}$ positions through electrochemistry.[90−92] All orbital energies are reported with respect to vacuum.

(Figure 1A) when the OLA-passivated nanocrystals are treated with $Cd(O_2CPh)_2$.

Mechanism (iii): Relaxation of Exciton Confinement. The various experimental approaches described above suggest that delocalization of exciton wave functions beyond the inorganic core boundary and formation of extended states occur upon $Cd(O_2CPh)_2$ attachment to OLA-passivated $(CdSe)_{34}$ nanocrystals. In the case of strongly confined (ultrasmall size) nanocrystals, the Coulombic interaction energy of the electron−hole pair is smaller than the kinetic energy of the electron and hole.[48,78] Thus, strongly confined exciton wave functions can potentially leak through the nanocrystal core boundary into the ligand monolayer, which results in an effective extension of the crystal lattice and expansion of the confinement box size. To better explain $Cd(O_2CPh)_2$-induced wave function delocalization of OLA-passivated $(CdSe)_{34}$ nanocrystals, we propose the simple MO diagram shown in Figure 6. The LUMOs of OLA-passivated $(CdSe)_{34}$ nanocrystals are Cd in character and when they are half-filled (in the excited state) they behave as electron donors that can interact with the LUMOs of the $Cd(O_2CPh)_2$ ligand, which is an electron acceptor. In the case of ultrasmall nanocrystals, a relatively large number of surface occupied orbitals are available, making the cumulative electronic interaction with ligand MOs very strong. For simplicity we illustrate only a single LUMO−LUMO interaction as shown in Figure 6A. We use the LUMO energy value of −3.19 eV (vs vacuum) for 1.6 nm diameter CdSe nanocrystals from literature reports of electrochemical measurements and an effective mass approximation calculation.[90−92] We determine the HOMO (−7.34 eV) and LUMO (−1.70 eV) energies of $Cd(O_2CPh)_2$ from geometry optimized density functional theory (DFT) calculations (LANL2DZ effective core potential for Cd^{2+} with the matching 6-311G** basis set and the B3LYP functional).

The interaction at the nanocrystal-$Cd(O_2CPh)_2$ interface creates new hybrid bonding and antibonding MOs in which electrons from the nanocrystal LUMO could delocalize into the newly formed hybrid bonding MO as illustrated in Figure 6B.[93]

As reported in the literature, in the steady state, the wave function of the exciton can delocalize into the interfacial orbitals, which facilitates an increase in the effective confinement boundary that in turn, results in a red-shift in the lowest energy absorption and band-edge emission peaks, and a change in τ_r.[11] In our system exciton delocalization from the LUMOs of ligand-passivated $(CdSe)_{34}$ nanocrystals into hybrid bonding MOs is facilitated by the extended π-conjugated electronic structure of the $Cd(O_2CPh)_2$ ligand. Although the nanocrystal-Cd(nanoanoate)$_2$ interaction potentially creates new hybrid bonding and antibonding MOs, π-conjugation is not present in Cd(nanoanoate)$_2$ to enable the delocalization of exciton wave functions in essence not increasing the size of the confinement box. Lack of conjugation is reflected in the absence of absorption and emission peak shifts.

When we consider the orbital mixing between the nanocrystal and its surface ligand, which results in formation of hybrid states,[94] it is important to recognize that not only the energy difference between them but also the their coupling constant control the extent of interaction. Here, the higher the coupling strength, the stronger the delocalization for a fixed energy difference.[44] In the context of perturbation theory, the interaction is expected to be different for different ligands (e.g., $Cd(O_2CPh)_2$ and Cd(nanoanoate)$_2$). For simplicity, we show only the interaction between one LUMO of the nanocrystal and one LUMO of the ligand (Figure 6A), but the LUMOs of the nanocrystal could interact with multiple LUMOs of $Cd(O_2CPh)_2$.[93] Moreover, these newly formed hybrid states composed of both nanocrystal and ligand are spread over both nanocrystal and ligand atoms, through which exciton (presumably electron) wave function delocalization takes place (Figure 6B). However, these complex electronic interactions require a more detailed computational study to model both the nanocrystal and ligands simultaneously.[67,94,95] This level of quantitative energy level calculation requires complex computational modeling and sophisticated DFT calculations, which are beyond our expertise.

Table 1. Shifts in the Lowest Energy Absorption and Emission Peak Positions, Emission Quantum Yields, and Fluorescence Lifetimes of OLA-Passivated (CdSe)$_{34}$ Nanocrystals after Treatment with Various Z-Type Ligands

ligand	absorption peak shift (nm)[a]	absorption peak shift (meV)	emission peak shift (nm)[a]	emission peak shift (meV)	quantum yield (%)[b]	PL lifetime (τ) (ns)[b,c]
Cd(benzoate)$_2$	36 ± 3	240 ± 12	43 ± 2	260 ± 9	70 ± 3	45.5 ± 7
Cd(nonanoate)$_2$	0	0	0	0	46 ± 6	39.1 ± 4.5
Cd(oleate)$_2$	11 ± 2	77 ± 4	16 ± 3	101 ± 12	18 ± 4	17.4 ± 2.3

[a]OLA-passivated (CdSe)$_{34}$ nanocrystals display lowest energy absorption and emission peaks at 416 and 435 nm, respectively. [b]The PLQY and PL lifetime of OLA-passivated (CdSe)$_{34}$ nanocrystals are 5% and 13.7 ns, respectively. [c]A stretch exponential function was used to determine the excited state lifetimes (see Experimental Section). For each metal-carboxylate, three different batches of OLA-passivated (CdSe)$_{34}$ nanocrystals were characterized after surface treatment to determine the average value and statistical deviation.

Finally, we also investigated the photophysical properties of OLA-passivated (CdSe)$_{34}$ nanocrystals upon treatment with Cd(oleate)$_2$ to determine its effect on the exciton delocalization process. We use very similar experimental conditions to those described for the other two Cd(carboxylate)$_2$ complexes to bind Cd(oleate)$_2$. Within 5 min we observe an 11 nm (77 ± 4 meV) red-shift in the lowest energy absorption peak and a 16 nm (101 ± 12 meV) red-shift in the band-edge emission peak (see Figure S10). Our PLQY is 18%, which is much lower than what we observe with either Cd(nonanoate)$_2$- or Cd(O$_2$CPh)$_2$-treated (CdSe)$_{34}$ nanocrystals. Table 1 provides a detail comparison of the photophysical properties of the three different Cd(carboxylate)$_2$ complexes. Importantly, the emission spectrum of Cd(oleate)$_2$-treated, OLA-passivated (CdSe)$_{34}$ nanocrystals contains both band-edge and broad-band features, which implies the presence of radiative surface midgap trap states, which are commonly observed for ultrasmall nanocrystals.[7,55,84] The FTIR analysis (Figure S11) shows that the original OLA ligand is nearly completely replaced by Cd(oleate)$_2$ similar to the previous reports by the Buhro and Owen groups.[25,50] In addition, the literature reports that magic-sized (CdSe)$_{34}$ nanocrystals are thermodynamically very stable, thus changes in the crystal structure and/or strain state are unlikely to occur, which further supports our Cd(nonanoate)$_2$ data in which no change in the lowest energy absorption peak is observed. Therefore, the apparent red-shift in the absorption and band-edge emission peaks after treatment of Cd(oleate)$_2$ is due to a combination of induced lattice strain and minor delocalization of the exciton wave function. This combination is in agreement with the work by the Buhro group.[50]

Dual Role of Z-Type Ligands: Passivation of Trap States and Exciton Delocalization. Our experimental emission data show that binding of Cd(O$_2$CPh)$_2$ to OLA-passivated (CdSe)$_{34}$ nanocrystals (1) red-shifts the band-edge emission peak, (2) increases the PLQY up to 14-fold, (3) increases the PL lifetime (τ) by 3.3 fold (Figure 7), and (4) increases k_r (calculated from the PLQY and τ) by 4.2 fold. The increase in PLQY and τ values for Cd(nonanoate)$_2$ nanocrystals is predominantly due to passivation of surface trap states. Thus, for Cd(O$_2$CPh)$_2$-treated nanocrystals with the exception of the red-shift of the band-edge emission peak, which results solely from delocalization of exciton wave functions, the other three emission components are modulated by a combination of nonradiative trap states passivation and electron wave function delocalization. However, it is difficult to quantitate the exact contribution from delocalization and surface trap state passivation. Specifically, it is reported in the literature that upon deposition of a ZnS shell, delocalization of exciton (electron and/or hole) wave functions increases the PLQY and τ for CdSe nanocrystals.[51] In a previous study of surface ligand-
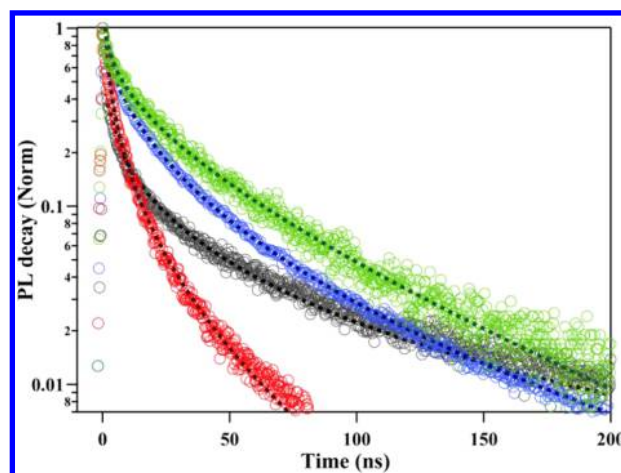

Figure 7. Photoluminescence lifetime decay of purified OLA-passivated (CdSe)$_{34}$ nanocrystals (red circles), after treatment with Cd(oleate)$_2$ (gray circles), Cd(nonanoate)$_2$ (blue circles), and Cd(O$_2$CPh)$_2$, (green circles). A stretch exponential function (dotted black lines) was used to fit the decay curves.

induced enhancement of PLQY of CdSe nanocrystals, Weiss and co-workers rationalized the enhancement as a consequence of an increase in the integrated extinction of the first excitonic transition.[11] Perhaps, ligands induce exciton delocalization of OLA-passivated (CdSe)$_{34}$ nanocrystals can be compared to core–shell nanocrystals where the inorganic shell is replaced by the organic monolayer, which is able to propagate the exciton wave functions.

According to Green's covalent bond theory, OLA is a neutral 2-electron donating L-type ligand, which passivates the surface Cd sites. The unpassivated Se sites, therefore, result in formation of midgap trap states, which enable capture of photogenerated electrons before they can radiatively recombine with holes at the edge of the HOMO, consequently causing low PLQY and τ. In the case of ultrasmall semiconductor nanocrystals (<2.0 diameter), the majority of the atoms (~90%) are at the surface, and thus a large number of surface occupied orbitals are available to capture the electrons if they are not fully passivated acting as nonradiative trap states.[49,96] This is a potential drawback for ultrasmall CdSe nanocrystals causing their weak emission properties.[8,52,55–57,59,61,65,66,68,84,85] Passivation of Se sites by 2-electron accepting Z-type ligands (e.g., metal-carboxylates) prevents the formation of midgap trap states. Therefore, fully passivated CdSe nanocrystals (with the surface Cd and Se sites passivated by L-type and Z-type ligands, respectively) are expected to exhibit much improved emission properties, as shown for our OLA-passivated (CdSe)$_{34}$

nanocrystals after surface attachment of metal-carboxylate complexes (see Table 1).

The PLQY contributions from delocalization of exciton wave functions versus passivation of midgap trap states by Cd-$(O_2CPh)_2$, was determined as shown by Jin et al.,[11] using our Cd(nonanoate)$_2$ values for reference because the structure lacks exciton delocalization. Our results strongly support the idea that ~25% of the increase in PLQY by treatment with $Cd(O_2CPh)_2$ is associated with excitonic wave function delocalization. Moreover, mixed OLA- and $Cd(O_2CPh)_2$-passivated $(CdSe)_{34}$ nanocrystals display a k_r of 15.6×10^6 s^{-1} in comparison to 3.7×10^6 s^{-1} found with only OLA-passivated nanocrystals. We should mention that the k_r value is a somewhat crude approximation given how the PL properties were characterized under our experimental conditions. Furthermore, the nonradiative rate constant (k_{nr}) of OLA-passivated $(CdSe)_{34}$ nanocrystals before and after $Cd(O_2CPh)_2$ treatment is determined to be 69.5×10^6 s^{-1} and 6.4×10^6 s^{-1}, respectively. Therefore, passivation of Se sites on $(CdSe)_{34}$ nanocrystals not only enhances the k_r but also reduces k_{nr} by 10-fold. Table S2 summarizes the various emission properties of $(CdSe)_{34}$ nanocrystals upon treatment with various Cd-(carboxylate)$_2$ complexes.

It is important to mention that the expression which both we and Jin et al.[11] have used is a somewhat crude approximation to determine the k_r by using $PLQY/\tau$, specifically for an ensemble measurement. The reason is 2-fold: (1) The ensemble PLQY is mostly determined by "dark nanocrystals" that are invisible in the PL decay experiment. Their presence causes the PLQY measurement to be low. (2) The PL decay experiment shows the decay dynamics of the bright nanocrystals only.[97] The observed radiative lifetime (see Table S2) for mixed OLA- and $Cd(O_2CPh)_2$-passivated $(CdSe)_{34}$ nanocrystals is exceedingly high compared to larger CdSe nanocrystals (>2.0 nm diameter) with their PLQY of 100% yielding a radiative lifetime of 20–30 ns as reported by Gao et al.[98] This discrepancy is because in our ensemble experiment, the contribution from the dark fraction has not been taken into consideration. Perhaps, a more systematic approach (including possibly a single nanocrystal PL study) as shown by Park et al.[99] is required to fully characterize the influence on k_r and radiative lifetime controlled by the surface ligand chemistry of metal chalcogenide nanocrystals.

The dual role of $Cd(O_2CPh)_2$ was further investigated through determination of the apparent increase in the excitonic radius ("delocalization radius", ΔR) of $(CdSe)_{34}$ nanocrystals with $Cd(O_2CPh)_2$ binding and its relationship to their PL emission. The ΔR values are determined from the time-dependent absorption spectra of OLA-passivated $(CdSe)_{34}$ nanocrystals after their treatment with $Cd(O_2CPh)_2$ at room temperature (see Figure 8A and Figure S12). As illustrated in Figure 8B, the PL/PL_0 ratio—PL is the time-dependent integrated band-edge emission intensity of the OLA-passivated $(CdSe)_{34}$ nanocrystals after treatment of $Cd(O_2CPh)_2$ and PL_0 is the emission intensity before treatment—monotonically increases with ΔR up to a value of ~30. This value of 30 is in agreement with the extent of enhancement of PLQY as discussed above. Therefore, the remaining enhancement in the band-edge peak position intensity is caused by the passivation of midgap trap states. A similar relationship (PL/PL_0 versus ΔR) was reported in the literature for X-type ligand passivation of larger CdSe nanocrystals (>2.0 nm diameter), in which the changes in emission properties are correlated with the delocalization of excitonic wave functions.[11] However, the
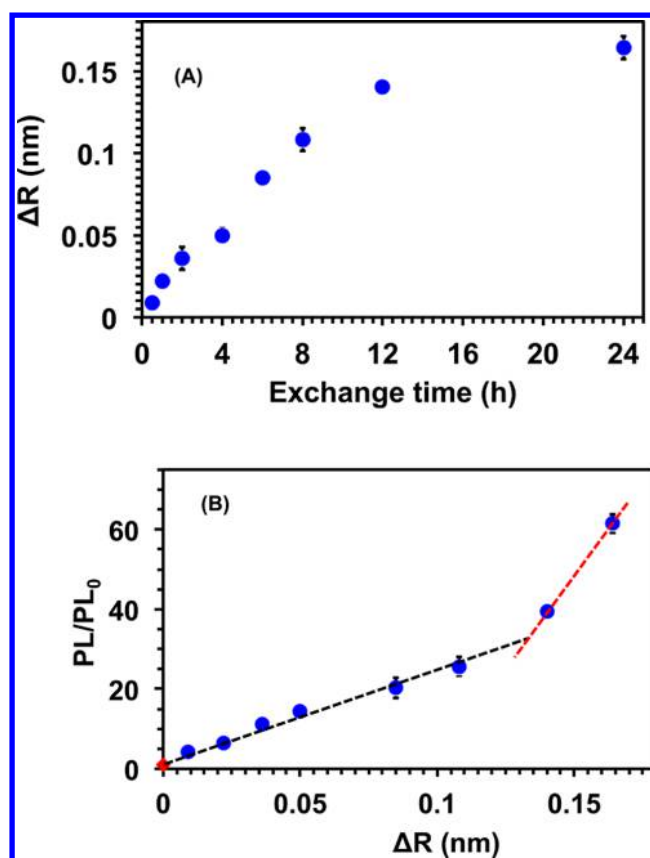

Figure 8. (A) Plot of the apparent increase of the excitonic radius (ΔR) of OLA-passivated $(CdSe)_{34}$ nanocrystals with time after exposure to $Cd(O_2CPh)_2$ at room temperature. The R values are determined using an empirical equation.[80] (B) Plot of enhancement of band-edge PL peak intensity of OLA-passivated $(CdSe)_{34}$ nanocrystals treated with $Cd(O_2CPh)_2$ as a function of calculated delocalization radius. Optical density of the nanocrystal solution at the excitation wavelength (380 nm) was kept constant.

effects of exciton wave function delocalization on emission properties of ultrasmall CdSe nanocrystals are more dramatic than those found with larger nanocrystals (>2.0 nm diameter). The proposed theory by Weiss and co-workers[11] underlying exciton delocalization into the ligand monolayer leading to increase in PLQY is complicated, but knowledge of electronic interactions between nanocrystals and ligands are critical for modulation of electronic properties.

Taken together, enhancement of PLQY and increase in k_r result from the attachment of $Cd(O_2CPh)_2$ onto the surface of $(CdSe)_{34}$ nanocrystals. Changes in these optoelectronic properties are induced by a combination of delocalization of exciton wave functions and elimination of nonradiative decay channels with the later component originating from the surface traps, which are inhibited by attachment of surface ligands. Therefore, in this present investigation, we demonstrate a dual role for the surface ligand $Cd(O_2CPh)_2$. Perhaps, we can compare such ligand attachment and passivation of the surface of our nanocrystals to core–shell nanocrystal with their high emission efficiencies.[100−103] In our case the semiconducting inorganic shell (e.g., CdS or ZnS) is replaced by the metal-carboxylate complex. Here one would expect to achieve an unprecedented modulation of photophysical properties of semiconductor nanocrystals through appropriate selection of surface ligand chemistry in which energetic alignment between

MOs of the nanocrystal and surface ligand would allow delocalization of exciton wave functions from the nanocrystal into the ligand monolayer. Furthermore, the exciton (electron and/or hole) wave function delocalization into the ligand monolayer depends strongly on the energetic coupling of interfacial orbitals between the nanocrystal and surface passivating ligands, that in turn, is influenced by definable (synthesizable) structural parameters of the metal(carboxylate)$_2$ complex. Further investigation of the effects of organic ligand chemical structure and group II metal identity is currently underway.

CONCLUSIONS

Unprecedentedly large bathochromic shifts of the lowest energy absorption and emission peaks of molecule-like (CdSe)$_{34}$ nanocrystals are observed upon treatment with Cd(O$_2$CPh)$_2$ by changing the surface ligand chemistry without changing the crystallographic structure of the original nanocrystals. The absorption and emission peaks are found to be reversible for at least five cycles of attachment and detachment of surface-bound Cd(O$_2$CPh)$_2$. On the basis of several control experiments, additional structural characterizations, and energy level calculations of three different Cd(carboxylate) complexes via DFT, we propose a MO diagram that shows delocalization of excitonic electron wave functions from nanocrystals into their interfacial electronic states, which are formed through interaction between LUMO of nanocrystal and LUMO of passivating ligand. Such delocalization is facilitated by the high kinetic energy of the exciton in the strong confinement region. Moreover, the Z-type ligands are responsible for substantial enhancement of the emission properties of ultrasmall semiconductor nanocrystals through simultaneous passivation of nonradiative trap states and exciton delocalization, demonstrating that Cd(O$_2$CPh)$_2$ performs a dual role in this process.

The intrinsic simplicity of the (CdSe)$_{34}$ crystal structure,[60,61,95] its large surface-to-volume ratio, and potential to provide electronic information at the molecular level, coupled with our finding of the simultaneous relaxation of exciton confinement and enhancement of emission properties will together allow the study of more complex photophysical properties (biexciton generation, Auger recombination, and exciton fine structure dynamics),[104−107] which are extremely challenging in the larger quantum dot systems. We predict that our large band gap tuning of ultrasmall CdSe nanocrystals will be applicable to other ultrasmall semiconductor nanocrystals (e.g., CdS, ZnS, and ZnSe) including those which are anisotropically shaped and strongly confined.[79,108−111]

Importantly, nanocrystal shape controls the overall geometry and symmetry of wave functions, polarization, and localization of electronic states.[112] Therefore, the degree of exciton delocalization arising from the interaction between the MOs of nanocrystals and surface passivating ligands will vary with change in nanocrystals shape. As a proof-of-concept, we investigated the exciton delocalization-induced band gap modulation of CdSe quantum wires and platelets, and CdS quantum platelets by treating their colloidal solution with Cd(O$_2$CPh)$_2$ at room temperature. We observe red-shifts of nearly 210, 265, and 150 nm in the lowest energy absorption peak for CdSe quantum wires, CdSe quantum platelets, and CdS quantum platelets, respectively (data not shown). We hypothesize that these wavelength shifts are due to an apparent geometry-specific, ligand binding-induced increase in the confinement box size and enhanced exciton delocalization,

and certainly the magnitude of delocalization varies strongly with geometry (CdSe quantum wires versus platelets) and composition (CdSe versus CdS quantum platelets). However, a thorough investigation is required to support our explanation, as is currently under examination and will be published separately. Nevertheless, modulation of exciton delocalization phenomena of these anisotropically shaped nanocrystals through manipulation of their surface ligand chemistry will not only shift the band gap from ultraviolet to the mid visible region of the solar spectrum, but also facilitate the charge transfer processes. In doing so, potential application of strongly confined nanocrystals to solar energy production will likely be enhanced.

EXPERIMENTAL SECTION

Materials. Cadmium acetate dihydrate (Cd(OAc)$_2$·2H$_2$O) (98%), cadmium oxide (99.99%), benzoic acid (99.5%), benzoic anhydride (95%), tetrahydrofuran (THF) (99.9%), oleic acid (99%), nonanoic acid (>96%), oleylamine (OLA) (70%), (1-hexanethiol (HT) (95%), toluene (HPLC grade), selenium (99.99%), N,N,N′,N′-tetramethyl-ethane-1,2-diamine (98%) (TMEDA), acetonitrile (MeCN) (HPLC grade), chloroform (HPLC grade), dichloromethane (DCM) (>99%), hexanes (95%), hexadecylamine (HDA) (90%), and trioctylphosphine (TOP) (90%) were purchased from Aldrich and used without further purification. Cadmium stearate (90%) was purchased from STREM Chemicals and used without purification. Methanol (99.98%) was purchased from Fisher Scientific.

Absorbance, NMR, and FTIR Spectroscopy, and Electron Microscopy Measurements. UV−vis absorption spectra were collected using a Varian Cary 50 UV−vis spectrophotometer over a range of 800−300 nm. Prior to sample measurement, the baseline was corrected using pure solvent. ^{1}H NMR was recorded on a Bruker AVANCE III 500 instrument at 500 MHz frequency. Approximately ∼10 mg of nanocrystals were dissolved in 0.6 mL of CD$_2$Cl$_2$ at room temperature and a minimum of 1000 scans were collected. A 15 s relaxation delay time was used, which is considered to be sufficient for accurate integration of the phenyl peak region.[113,114] FTIR spectra were acquired using a Thermo Nicolet IS10 FTIR spectrometer. For FTIR analysis, samples were prepared using a 1:10 ratio of sample to KBr, ground using a mortar and pestle, and pressed into a pellet. A minimum of 300 scans were collected and all data was processed using Omnic FTIR software.

The PLQYs of the synthesized OLA-passivated (CdSe)$_{34}$ nanocrystals before and after Z-type ligand attachments were calculated via a comparison technique using coumarin-30 as a standard fluorophore. Coumarin-30 exhibits a UV−vis absorption maximum at 407 nm and an emission maximum at 482 nm when excited at 380 nm with a QY of 55.3% in acetonitrile.[115] All samples were prepared in toluene and the optical density of the samples was kept to a similar level (∼0.08−0.1 peak absorption intensity). The emission data were collected from 400 to 700 nm and the area of the PL peak was determined. The following equation was used to calculate the PLQY of the (CdSe)$_{34}$ nanocrystals:[68]

$$\text{PLQY}_{NC} = \left(\frac{E_{NC}/A_{NC}}{E_{STD}/A_{STD}} \right) \times \left(\frac{\eta_{NC}}{\eta_{STD}} \right)^2 \times (\text{PLQY})_{STD} \tag{1}$$

Here PLQY$_{NC}$, A_{NC}, and E_{NC} represent the calculated quantum yield at 380 nm excitation wavelength, measured absorbance, and integrated emission intensity of the (CdSe)$_{34}$ nanocrystals, respectively. PLQY$_{STD}$ is the quantum yield of coumarin-30 and the η values refer to the refractive indices of the two solvents.

We also determined the PLQY of (CdSe)$_{34}$ nanocrystals using quinine sulfate (in 0.1 M H$_2$SO$_4$) as a standard fluorophore (PLQY$_{STD}$ = 54% at 350 nm excitation wavelength)[116] using eq 1. The PLQYs of Cd(O$_2$CPh)$_2$-treated (CdSe)$_{34}$ nanocrystals were 70 and 63% with respect to coumarin-30 and quinine sulfate, respectively. This slight variation in PLQY for two different standard fluorophore could be due

to differences in the excitation wavelengths. To the best of our knowledge, the PLQY achieved for our Cd(O$_2$CPh)$_2$-treated (CdSe)$_{34}$ nanocrystals is the highest value reported for such an ultrasmall CdSe nanocrystals.[7,52−55,84]

Ground State Photoluminescence, Excited State Lifetime, and Absolute Quantum Yield Measurement. The photoluminescence emission (PL) spectra were acquired using a Cary Eclipse fluorescence spectrophotometer from Varian Instruments. The lifetime measurements were recorded using a Time-correlated single photon counting (TCSPC) experimental set up. The data acquisition card (DAQ) was from Edinburgh Instrument (TCC900). The laser was a 405 nm pulsed laser from PICOQUANT (LDH-D-C-405M, CW-80 MHz) with pulse width <100 ps. The detector was a photomultiplier tube (PMT) from HAMAMATSU (H7422−40). The samples were excited at maximum absorption wavelength and the lifetime decay was measured at the emission wavelength maximum. The following stretch exponential equation[117] was employed to determine the excited state lifetime using the data obtained from the TCSPC experimental set up:

$$I(t) = I_0 \exp\left[-\left(\frac{t}{\tau}\right)^{\beta}\right] \tag{2}$$

Here $I(t)$ and I_0 are the PL intensities at time t and zero. β and τ are the dispersion factor and emission decay time, respectively. For the limiting case where $\beta \to 1$, a single exponential decay was observed with a characteristic lifetime of τ.

Synthesis of Cd(O$_2$CPh)$_2$. Cd(O$_2$CPh)$_2$ was synthesized using a literature procedure with minor modifications.[118] Briefly, 6.0 g (47 mmol) of cadmium oxide, 34.4 g (282 mmol) of benzoic acid, and 12.7 g (56 mmol) of benzoic anhydride were combined in a Schlenk flask and stirred under N$_2$ at 180 °C until a colorless melt appeared. The clear viscous liquid was allowed to cool to room temperature while stirring and then 100 mL toluene was added. To remove unreacted products, the solid was collected on a fritted filter while washing with toluene (3 × 200 mL) and DCM (3 × 200 mL). The white powder was redissolved in a mixture of 1:3 THF to DCM in a round-bottom flask, and the solution was concentrated by rotary distillation. The resulting milky white suspension was then filtered again and washed with a copious amount of a 1:1 mixture of DCM and toluene (3 × 100 mL). The white powder was dried under high vacuum at 100 °C overnight. Yield: 6.52 g (79%). The product purity was determined using ^{1}H NMR. Cadmium nonanoate was synthesized using a previously published procedure.[119] Cd(oleate)$_2$ was synthesized using the similar protocol as described in the literature.[50] The product was obtained through precipitation by dropwise addition of acetone. The product was centrifuged for 5 min at 7000 rpm and the clear supernatant was discarded. The purified Cd(oleate)$_2$ was dried under vacuum overnight.

Synthesis of OLA-Passivated (CdSe)$_{34}$ Nanocrystals. OLA-passivated (CdSe)$_{34}$ nanocrystals were synthesized using our published procedure with minor modifications.[7] Briefly, 0.2 g of Cd(OAc)$_2$·2H$_2$O was dissolved in 5 mL of OLA in a 100 mL two-neck round-bottom flask under reduced pressure while stirring. The Se precursor was prepared by adding 0.12 g of freshly ground selenium powder to a 5 mL round-bottom flask with 1.57 mL OLA and 0.430 mL of HT under N$_2$ atmosphere and stirring until all the Se was dissolved. Once a clear solution of Cd salt was achieved, 5 mL toluene was added to the reaction mixture. Then, 1 mL of the freshly prepared Se precursor was added to the mixture and then stirred for 24 h under N$_2$ atmosphere. The nanocrystals growth was quenched by diluting with 20 mL of hexane and adding a mixture of acetonitrile/methanol (1:1 v/v) dropwise until the solution become cloudy. The solution was then centrifuged at 7000 r.p.m. for 5 min yielding a yellow solid. The purification step was repeated an additional two times to remove free ligand. The resulting nanocrystals were used in the present investigation.

Synthesis of Cd(stearate)$_2$ Passivated (CdSe)$_{34}$ Nanocrystals. Nanocrystals were synthesized using a literature procedure.[85] Briefly, 0.56 g of cadmium stearate (0.5 mmol) was mixed with 9.66 g of hexadecylamine (HDA) (40.0 mmol) in a 25 mL Schlenk flask and heated at 100 °C under N$_2$. When a clear viscous colorless liquid appeared, 1.0 mL of TOPSe (1 mmol) stock solution was swiftly injected. TOPSe precursor was prepared inside a N$_2$ filled glovebox. The reaction was allowed to proceed at this temperature and then it was diluted in 25 mL chloroform and finally ethanol was added dropwise until cloudy. The solution was centrifuged for 5 min at 7000 rpm. The resulting yellow solid was dissolved in chloroform and used immediately.

Postsynthetic Surface Modification of CdSe Nanocrystals with Cd(O$_2$CPh)$_2$. A 10 mL 0.25 mM homogeneous stock solution of OLA-passivated (CdSe)$_{34}$ nanocrystals was prepared in toluene. To the solution, 0.25 g (0.7 mmol) of solid Cd(O$_2$CPh)$_2$ was added. The biphasic reaction mixture was stirred under N$_2$ atmosphere for 24 h and then centrifuged to remove any free Cd(O$_2$CPh)$_2$. Next, acetone was added dropwise to form a turbid solution, which was then centrifuged and the solid collected. The yellow solid was dissolved in toluene for spectroscopy and microscopy characterizations. Postsynthetic surface modification of with Cd(nonanoate)$_2$ and Cd(oleate)$_2$ was conducted under identical experimental conditions as Cd(O$_2$CPh)$_2$.

Modification of Cd(O$_2$CPh)$_2$: Treated CdSe Nanocrystals through Displacement by TMEDA. A homogeneous 0.25 mM stock solution of the OLA-passivated Cd(O$_2$CPh)$_2$-treated (CdSe)$_{34}$ nanocrystals was prepared in 10 mL toluene. Then 0.52 mL (0.03 mmol) of TMEDA was added while stirring under N$_2$ atmosphere for 1 h at room temperature. The displacement of the Cd(O$_2$CPh)$_2$)was monitored using UV−visible, PL, ^{1}H NMR, and FTIR spectroscopy.

Rebinding of Cd(O$_2$CPh)$_2$. After displacing Cd(O$_2$CPh)$_2$ through TMEDA treatment, (CdSe)$_{34}$ nanocrystals were precipitated by adding acetone. Then 0.25 g (0.7 mmol) Cd(O$_2$CPh)$_2$ was added and stirred overnight. The nanocrystals were purified through centrifugation and solvent-assisted precipitation, as mentioned above.

Theoretical Calculation of HOMO and LUMO Energy Position. Orbital energy calculations were performed with QChem 3.1 software using a LANL2DZ effective core potential for Cd^{2+} with the matching basis set of 6-311+G** and B3LYP functional.

■ ASSOCIATED CONTENT

ⓈSupporting Information

The Supporting Information is available free of charge on the ACS Publications website at DOI: 10.1021/jacs.6b04888.

> UV−visible absorption, photoluminescence, ^{1}H NMR, and FTIR spectra of various ligand-passivated (CdSe)$_{34}$ nanocrystals, HRTEM images of OLA-passivated (CdSe)$_{34}$ nanocrystals before and after Cd(O$_2$CPh)$_2$ treatment, solution stability of mixed OLA- and Cd(O$_2$CPh)$_2$-passivated (CdSe)$_{34}$ nanocrystals, and additional DFT calculation. (PDF)

■ AUTHOR INFORMATION

Corresponding Author

*rsardar@iupui.edu

Notes

The authors declare no competing financial interest.

■ ACKNOWLEDGMENTS

■ REFERENCES

(1) Hines, D. A.; Kamat, P. V. *ACS Appl. Mater. Interfaces* **2014**, *6*, 3041−3057.

(2) Chen, O.; Yang, Y.; Wang, T.; Wu, H.; Niu, C.; Yang, J.; Cao, Y. C. *J. Am. Chem. Soc.* **2011**, *133*, 17504−17512.

(3) Kuno, M.; Lee, J. K.; Dabbousi, B. O.; Mikulec, F. V.; Bawendi, M. G. *J. Chem. Phys.* **1997**, *106*, 9869−9882.

(4) Munro, A. M.; Jen-La Plante, I.; Ng, M. S.; Ginger, D. S. *J. Phys. Chem. C* **2007**, *111*, 6220−6227.

(5) Wei, H. H.-Y.; Evans, C. M.; Swartz, B. D.; Neukirch, A. J.; Young, J.; Prezhdo, O. V.; Krauss, T. D. *Nano Lett.* **2012**, *12*, 4465−4471.

(6) Krause, M. M.; Mooney, J.; Kambhampati, P. *ACS Nano* **2013**, *7*, 5922−5929.

(7) Dolai, S.; Nimmala, P. R.; Mandal, M.; Muhoberac, B. B.; Dria, K.; Dass, A.; Sardar, R. *Chem. Mater.* **2014**, *26*, 1278−1285.

(8) Rosson, T. E.; Claiborne, S. M.; McBride, J. R.; Stratton, B. S.; Rosenthal, S. J. *J. Am. Chem. Soc.* **2012**, *134*, 8006−8009.

(9) Baker, D. R.; Kamat, P. V. *Langmuir* **2010**, *26*, 11272−11276.

(10) Bullen, C.; Mulvaney, P. *Langmuir* **2006**, *22*, 3007−3013.

(11) Jin, S.; Harris, R. D.; Lau, B.; Aruda, K. O.; Amin, V. A.; Weiss, E. A. *Nano Lett.* **2014**, *14*, 5323−5328.

(12) Kongkanand, A.; Tvrdy, K.; Takechi, K.; Kuno, M.; Kamat, P. V. *J. Am. Chem. Soc.* **2008**, *130*, 4007−4015.

(13) Robel, I.; Subramanian, V.; Kuno, M.; Kamat, P. V. *J. Am. Chem. Soc.* **2006**, *128*, 2385−2393.

(14) Gur, I.; Fromer, N. A.; Geier, M. L.; Alivisatos, A. P. *Science* **2005**, *310*, 462−465.

(15) Huynh, W. U.; Dittmer, J. J.; Alivisatos, A. P. *Science* **2002**, *295*, 2425−2427.

(16) Tisdale, W. A.; Williams, K. J.; Timp, B. A.; Norris, D. J.; Aydil, E. S.; Zhu, X. Y. *Science* **2010**, *328*, 1543−1547.

(17) Talapin, D. V.; Lee, J.-S.; Kovalenko, M. V.; Shevchenko, E. V. *Chem. Rev.* **2009**, *110*, 389−458.

(18) Law, M.; Luther, J. M.; Song, Q.; Hughes, B. K.; Perkins, C. L.; Nozik, A. J. *J. Am. Chem. Soc.* **2008**, *130*, 5974−5985.

(19) Liu, Y.; Tolentino, J.; Gibbs, M.; Ihly, R.; Perkins, C. L.; Liu, Y.; Crawford, N.; Hemminger, J. C.; Law, M. *Nano Lett.* **2013**, *13*, 1578−1587.

(20) Kovalenko, M. V.; Scheele, M.; Talapin, D. V. *Science* **2009**, *324*, 1417−1420.

(21) Steigerwald, M. L.; Brus, L. E. *Acc. Chem. Res.* **1990**, *23*, 183−188.

(22) Murray, C. B.; Norris, D. J.; Bawendi, M. G. *J. Am. Chem. Soc.* **1993**, *115*, 8706−8715.

(23) Qu, L.; Yu, W. W.; Peng, X. *Nano Lett.* **2004**, *4*, 465−469.

(24) Peng, X.; Manna, L.; Yang, W.; Wickham, J.; Scher, E.; Kadavanich, A.; Alivisatos, A. P. *Nature* **2000**, *404*, 59−61.

(25) Anderson, N. C.; Hendricks, M. P.; Choi, J. J.; Owen, J. S. *J. Am. Chem. Soc.* **2013**, *135*, 18536−18548.

(26) Green, M. *J. Organomet. Chem.* **1995**, *500*, 127−148.

(27) Jana, A.; Lawrence, K. N.; Teunis, M. B.; Mandal, M.; Kumbhar, A.; Sardar, R. *Chem. Mater.* **2016**, *28*, 1107−1120.

(28) Haram, S. K.; Quinn, B. M.; Bard, A. J. *J. Am. Chem. Soc.* **2001**, *123*, 8860−8861.

(29) Shim, M.; Guyot-Sionnest, P. *Nature* **2000**, *407*, 981−983.

(30) Wang, C.; Shim, M.; Guyot-Sionnest, P. *Science* **2001**, *291*, 2390−2392.

(31) Norman, Z. M.; Anderson, N. C.; Owen, J. S. *ACS Nano* **2014**, *8*, 7513−7521.

(32) Rosen, E. L.; Buonsanti, R.; Llordes, A.; Sawvel, A. M.; Milliron, D. J.; Helms, B. A. *Angew. Chem., Int. Ed.* **2012**, *51*, 684−689.

(33) Lee, J.-S.; Kovalenko, M. V.; Huang, J.; Chung, D. S.; Talapin, D. V. *Nat. Nanotechnol.* **2011**, *6*, 348−352.

(34) Talapin, D. V.; Murray, C. B. *Science* **2005**, *310*, 86−89.

(35) Yu, D.; Wang, C.; Guyot-Sionnest, P. *Science* **2003**, *300*, 1277−1280.

(36) Soo Choi, H.; Liu, W.; Misra, P.; Tanaka, E.; Zimmer, J. P.; Itty Ipe, B.; Bawendi, M. G.; Frangioni, J. V. *Nat. Biotechnol.* **2007**, *25*, 1165−1170.

(37) Medintz, I. L.; Uyeda, H. T.; Goldman, E. R.; Mattoussi, H. *Nat. Mater.* **2005**, *4*, 435−446.

(38) Bruchez, M.; Moronne, M.; Gin, P.; Weiss, S.; Alivisatos, A. P. *Science* **1998**, *281*, 2013−2016.

(39) Chan, W. C. W.; Nie, S. *Science* **1998**, *281*, 2016−2018.

(40) Peterson, M. D.; Cass, L. C.; Harris, R. D.; Edme, K.; Sung, K.; Weiss, E. A. *Annu. Rev. Phys. Chem.* **2014**, *65*, 317−339.

(41) Kalyuzhny, G.; Murray, R. W. *J. Phys. Chem. B* **2005**, *109*, 7012−7021.

(42) Omogo, B.; Aldana, J. F.; Heyes, C. D. *J. Phys. Chem. C* **2013**, *117*, 2317−2327.

(43) Frederick, M. T.; Weiss, E. A. *ACS Nano* **2010**, *4*, 3195−3200.

(44) Frederick, M. T.; Amin, V. A.; Swenson, N. K.; Ho, A. Y.; Weiss, E. A. *Nano Lett.* **2012**, *13*, 287−292.

(45) Xie, Y.; Teunis, M. B.; Pandit, B.; Sardar, R.; Liu, J. *J. Phys. Chem. C* **2015**, *119*, 2813−2821.

(46) Teunis, M. B.; Dolai, S.; Sardar, R. *Langmuir* **2014**, *30*, 7851−7858.

(47) Buckley, J. J.; Couderc, E.; Greaney, M. J.; Munteanu, J.; Riche, C. T.; Bradforth, S. E.; Brutchey, R. L. *ACS Nano* **2014**, *8*, 2512−2521.

(48) Brus, L. E. *J. Chem. Phys.* **1984**, *80*, 4403−4409.

(49) Brus, L. *J. Phys. Chem.* **1986**, *90*, 2555−2560.

(50) Zhou, Y.; Wang, F.; Buhro, W. E. *J. Am. Chem. Soc.* **2015**, *137*, 15198−15208.

(51) Mokari, T.; Banin, U. *Chem. Mater.* **2003**, *15*, 3955−3960.

(52) Dolai, S.; Dutta, P.; Muhoberac, B. B.; Irving, C. D.; Sardar, R. *Chem. Mater.* **2015**, *27*, 1057−1070.

(53) Wang, Y.; Zhang, Y.; Wang, F.; Giblin, D. E.; Hoy, J.; Rohrs, H. W.; Loomis, R. A.; Buhro, W. E. *Chem. Mater.* **2014**, *26*, 2233−2243.

(54) Bowers, I. M. J.; McBride, J. R.; Garrett, M. D.; Sammons, J. A.; Dukes Iii, A. D.; Schreuder, M. A.; Watt, T. L.; Lupini, A. R.; Pennycook, S. J.; Rosenthal, S. J. *J. Am. Chem. Soc.* **2009**, *131*, 5730−5731.

(55) Bowers, M. J.; McBride, J. R.; Rosenthal, S. J. *J. Am. Chem. Soc.* **2005**, *127*, 15378−15379.

(56) Evans, C. M.; Guo, L.; Peterson, J. J.; Maccagnano-Zacher, S.; Krauss, T. D. *Nano Lett.* **2008**, *8*, 2896−2899.

(57) Landes, C.; Braun, M.; Burda, C.; El-Sayed, M. A. *Nano Lett.* **2001**, *1*, 667−670.

(58) Riehle, F. S.; Bienert, R.; Thomann, R.; Urban, G. A.; Kruger, M. *Nano Lett.* **2009**, *9*, 514−518.

(59) Lawrence, K. N.; Dolai, S.; Lin, Y.-H.; Dass, A.; Sardar, R. *RSC Adv.* **2014**, *4*, 30742−30753.

(60) Nguyen, K. A.; Day, P. N.; Pachter, R. *J. Phys. Chem. C* **2010**, *114*, 16197−16209.

(61) Kasuya, A.; Sivamohan, R.; Barnakov, Y. A.; Dmitruk, I. M.; Nirasawa, T.; Romanyuk, V. R.; Kumar, V.; Mamykin, S. V.; Tohji, K.; Jeyadevan, B.; Shinoda, K.; Kudo, T.; Terasaki, O.; Liu, Z.; Belosludov, R. V.; Sundararajan, V.; Kawazoe, Y. *Nat. Mater.* **2004**, *3*, 99−102.

(62) Yu, K. *Adv. Mater.* **2012**, *24*, 1123−1132.

(63) Harrell, S. M.; McBride, J. R.; Rosenthal, S. J. *Chem. Mater.* **2013**, *25*, 1199−1210.

(64) Yu, K.; Hu, M. Z.; Wang, R.; Piolet, M. L.; Frotey, M.; Zaman, M. B.; Wu, X.; Leek, D. M.; Tao, Y.; Wilkinson, D.; Li, C. *J. Phys. Chem. C* **2010**, *114*, 3329−3339.

(65) Soloviev, V. N.; Eichhofer, A.; Fenske, D.; Banin, U. *J. Am. Chem. Soc.* **2000**, *122*, 2673−2674.

(66) Soloviev, V. N.; Eichhofer, A.; Fenske, D.; Banin, U. *J. Am. Chem. Soc.* **2001**, *123*, 2354−2364.

(67) Kilina, S.; Velizhanin, K. A.; Ivanov, S.; Prezhdo, O. V.; Tretiak, S. *ACS Nano* **2012**, *6*, 6515−6524.

(68) Newton, J. C.; Ramasamy, K.; Mandal, M.; Joshi, G. K.; Kumbhar, A.; Sardar, R. *J. Phys. Chem. C* **2012**, *116*, 4380−4389.

(69) Lawrence, K.; Johnson, M.; Dolai, S.; Kumbhar, A.; Sardar, R. *Nanoscale* **2015**, *7*, 11667−11677.

(70) Scheele, M.; Hanifi, D.; Zherebetskyy, D.; Chourou, S. T.; Axnanda, S.; Rancatore, B. J.; Thorkelsson, K.; Xu, T.; Liu, Z.; Wang, L.-W.; Liu, Y.; Alivisatos, A. P. *ACS Nano* **2014**, *8*, 2532–2540.

(71) Knowles, K. E.; Tice, D. B.; McArthur, E. A.; Solomon, G. C.; Weiss, E. A. *J. Am. Chem. Soc.* **2009**, *132*, 1041–1050.

(72) Micic, O. I.; Ahrenkiel, S. P.; Nozik, A. J. *Appl. Phys. Lett.* **2001**, *78*, 4022–4024.

(73) Koole, R.; Liljeroth, P.; de Mello Donega, C.; Vanmaekelbergh, D.; Meijerink, A. *J. Am. Chem. Soc.* **2006**, *128*, 10436–10441.

(74) Choi, J.-H.; Fafarman, A. T.; Oh, S. J.; Ko, D.-K.; Kim, D. K.; Diroll, B. T.; Muramoto, S.; Gillen, J. G.; Murray, C. B.; Kagan, C. R. *Nano Lett.* **2012**, *12*, 2631–2638.

(75) Crisp, R. W.; Schrauben, J. N.; Beard, M. C.; Luther, J. M.; Johnson, J. C. *Nano Lett.* **2013**, *13*, 4862–4869.

(76) Beard, M. C.; Turner, G. M.; Murphy, J. E.; Micic, O. I.; Hanna, M. C.; Nozik, A. J.; Schmuttenmaer, C. A. *Nano Lett.* **2003**, *3*, 1695–1699.

(77) Bryant, G. W.; Jaskolski, W. *Phys. E* **2002**, *13*, 293–296.

(78) Frederick, M. T.; Amin, V. A.; Cass, L. C.; Weiss, E. A. *Nano Lett.* **2011**, *11*, 5455–5460.

(79) Wang, Y.; Zhou, Y.; Zhang, Y.; Buhro, W. E. *Inorg. Chem.* **2015**, *54*, 1165–1177.

(80) Yu, W. W.; Qu, L.; Guo, W.; Peng, X. *Chem. Mater.* **2003**, *15*, 2854–2860.

(81) Badia, A.; Demers, L.; Dickinson, L.; Morin, F. G.; Lennox, R. B.; Reven, L. *J. Am. Chem. Soc.* **1997**, *119*, 11104–11105.

(82) Dolai, S.; Dass, A.; Sardar, R. *Langmuir* **2013**, *29*, 6187–6193.

(83) Cooper, J. K.; Franco, A. M.; Gul, S.; Corrado, C.; Zhang, J. Z. *Langmuir* **2011**, *27*, 8486–8493.

(84) Cossairt, B. M.; Owen, J. S. *Chem. Mater.* **2011**, *23*, 3114–3119.

(85) Kuçur, E.; Ziegler, J.; Nann, T. *Small* **2008**, *4*, 883–887.

(86) Fritzinger, B.; Capek, R. K.; Lambert, K.; Martins, J. C.; Hens, Z. *J. Am. Chem. Soc.* **2010**, *132*, 10195–10201.

(87) Hassinen, A.; Moreels, I.; De Nolf, K.; Smet, P. F.; Martins, J. C.; Hens, Z. *J. Am. Chem. Soc.* **2012**, *134*, 20705–20712.

(88) Morris-Cohen, A. J.; Frederick, M. T.; Lilly, G. D.; McArthur, E. A.; Weiss, E. A. *J. Phys. Chem. Lett.* **2010**, *1*, 1078–1081.

(89) Morris-Cohen, A. J.; Malicki, M.; Peterson, M. D.; Slavin, J. W. J.; Weiss, E. A. *Chem. Mater.* **2013**, *25*, 1155–1165.

(90) Querner, C.; Reiss, P.; Sadki, S.; Zagorska, M.; Pron, A. *Phys. Chem. Chem. Phys.* **2005**, *7*, 3204–3209.

(91) Wang, L.-W.; Zunger, A. *Phys. Rev. B: Condens. Matter Mater. Phys.* **1996**, *53*, 9579.

(92) Wang, L.-W.; Califano, M.; Zunger, A.; Franceschetti, A. *Phys. Rev. Lett.* **2003**, *91*, 056404–056407.

(93) Hoffmann, R. *Rev. Mod. Phys.* **1988**, *60*, 601–628.

(94) Kilina, S.; Ivanov, S.; Tretiak, S. *J. Am. Chem. Soc.* **2009**, *131*, 7717–7726.

(95) Prezhdo, O. V. *Acc. Chem. Res.* **2009**, *42*, 2005–2016.

(96) Hill, N. A.; Whaley, K. B. *J. Chem. Phys.* **1994**, *100*, 2831–2837.

(97) The authors thank the reviewer for bringing this to their attention.

(98) Gao, Y.; Peng, X. *J. Am. Chem. Soc.* **2015**, *137*, 4230–4235.

(99) Park, Y.-S.; Bae, W. K.; Pietryga, J. M.; Klimov, V. I. *ACS Nano* **2014**, *8*, 7288–7296.

(100) Smith, A. M.; Nie, S. *Acc. Chem. Res.* **2009**, *43*, 190–200.

(101) Hines, M. A.; Guyot-Sionnest, P. *J. Phys. Chem.* **1996**, *100*, 468–471.

(102) Garcia-Santamari, F.; Chen, Y.; Vela, J.; Schaller, R. D.; Hollingsworth, J. A.; Klimov, V. I. *Nano Lett.* **2009**, *9*, 3482–3488.

(103) Chen, O.; Zhao, J.; Chauhan, V. P.; Cui, J.; Wong, C.; Harris, D. K.; Wei, H.; Han, H.-S.; Fukumura, D.; Jain, R. K.; Bawendi, M. G. *Nat. Mater.* **2013**, *12*, 445–451.

(104) Cohn, A. W.; Schimpf, A. M.; Gunthardt, C. E.; Gamelin, D. R. *Nano Lett.* **2013**, *13*, 1810–1815.

(105) Ellingson, R. J.; Beard, M. C.; Johnson, J. C.; Yu, P.; Micic, O. I.; Nozik, A. J.; Shabaev, A.; Efros, A. L. *Nano Lett.* **2005**, *5*, 865–871.

(106) Johnson, J. C.; Gerth, K. A.; Song, Q.; Murphy, J. E.; Nozik, A. J.; Scholes, G. D. *Nano Lett.* **2008**, *8*, 1374–1381.

(107) Robel, I.; Bunker, B. A.; Kamat, P. V.; Kuno, M. *Nano Lett.* **2006**, *6*, 1344–1349.

(108) Ithurria, S.; Dubertret, B. *J. Am. Chem. Soc.* **2008**, *130*, 16504–16505.

(109) Joo, J.; Son, J. S.; Kwon, S. G.; Yu, J. H.; Hyeon, T. *J. Am. Chem. Soc.* **2006**, *128*, 5632–5633.

(110) Liu, Y.-H.; Wang, F.; Wang, Y.; Gibbons, P. C.; Buhro, W. E. *J. Am. Chem. Soc.* **2011**, *133*, 17005–17013.

(111) Zanella, M.; Abbasi, A. Z.; Schaper, A. K.; Parak, W. J. *J. Phys. Chem. C* **2010**, *114*, 6205–6215.

(112) Kim, J.; Nair, P. S.; Wong, C. Y.; Scholes, G. D. *Nano Lett.* **2007**, *7*, 3884–3890.

(113) Campos, M. P.; Owen, J. S. *Chem. Mater.* **2016**, *28*, 227–233.

(114) Tavasoli, E.; Guo, Y.; Kunal, P.; Grajeda, J.; Gerber, A.; Vela, J. *Chem. Mater.* **2012**, *24*, 4231–4241.

(115) Senthilkumar, S.; Nath, S.; Pal, H. *Photochem. Photobiol.* **2004**, *80*, 104–111.

(116) Chen, Y.; Zheng, M.; Xiao, Y.; Dong, H.; Zhang, H.; Zhuang, J.; Hu, H.; Lei, B.; Liu, Y. *Adv. Mater.* **2016**, *28*, 312–318.

(117) Shi, D.; Adinolfi, V.; Comin, R.; Yuan, M.; Alarousu, E.; Buin, A.; Chen, Y.; Hoogland, S.; Rothenberger, A.; Katsiev, K.; Losovyj, Y.; Zhang, X.; Dowben, P. A.; Mohammed, O. F.; Sargent, E. H.; Bakr, O. M. *Science* **2015**, *347*, 519–522.

(118) Beecher, A. N.; Yang, X.; Palmer, J. H.; LaGrassa, A. L.; Juhas, P.; Billinge, S. J. L.; Owen, J. S. *J. Am. Chem. Soc.* **2014**, *136*, 10645–10653.

(119) Zhang, L.-J.; Shen, X.-C.; Liang, H.; Yao, J.-T. *J. Phys. Chem. C* **2010**, *114*, 21921–21927.